Research Article

Does dentine mineral change with anatomical location, microscopic site and patient age?

Arosha T. Weerakoon [a,*], Crystal Cooper [b], Ian A. Meyers [a], Nicholas Condon [c], Christopher Sexton [a], David Thomson [a], Pauline J. Ford [a], Anne L. Symons [a]

[a] School of Dentistry, The University of Queensland, Brisbane, Queensland, Australia
[b] Central Analytical Research Facility, Queensland University of Technology, Brisbane, Queensland, Australia
[c] Institute for Molecular Bioscience, The University of Queensland, Brisbane, Queensland, Australia

ARTICLE INFO

ABSTRACT

Objective: To determine the effect of patient age (young or mature), anatomical location (shallow/deep and central/peripheral) and microscopic site (intertubular/peritubular) on dentine mineral density, distribution and composition.

Methods: Extracted posterior teeth from young (aged 19–20 years, N = 4) and mature (aged 54–77 years, N = 4) subjects were prepared to shallow and deep slices. The dentine surface elemental composition was investigated in a SEM using Backscattered Electron (BSE) micrographs, Energy Dispersive X-ray Spectroscopy, and Integrated Mineral Analysis. Qualitative comparisons and quantitative measures using machine learning were used to analyse the BSE images. Quantitative outcomes were compared using quantile or linear regression models with bootstrapping to account for the multiple measures per sample. Subsequently, a Xenon Plasma Focussed Ion Beam Scanning Electron Microscopy (Xe PFIB-SEM) was used to mill large area (100 μm) cross-sections to investigate morphology through the dentine tubules using high resolution secondary electron micrographs.

Results: With age, dentine mineral composition remains stable, but density changes with anatomical location and microscopic site. Microscopically, accessory tubules spread into intertubular dentine (ITD) from the main tubule lumens. Within the lumens, mineral deposits form calcospherites in the young that eventually coalesce in mature tubules and branches. The mineral occlusion in mature dentine increases overall ITD density to reflect peritubular dentine (PTD) infiltrate. The ITD observed in micrographs remained consistent for age and observation plane to suggest tubule deposition affects overall dentine density. Mineral density depends on the relative distribution of PTD to ITD that varies with anatomical location.

Significance: Adhesive materials may interact differently within a tooth as well as in different age groups.

Introduction

Globally, public health improvements have minimised tooth loss in ageing populations, to result in growing demand for complex management (Müller et al., 2017). In dentistry, complex yet conservative restorative treatment (Müller et al., 2017) involves replacing carious or fractured tooth tissue with adhesive materials (Eltahlah et al., 2018). Yet adhesive materials variably adapt to tooth tissue, particularly dentine (Blatz et al., 2019), and dentine mechanical properties change with patient age (Arola and Reprogel, 2005; Bajaj et al., 2006) or anatomical location and microscopic site (Chu et al., 2010; Mjör and Nordahl, 1996). Site, location and age-related changes are often studied and reported (Perdigao, 2010), yet no recent research has addressed the combined effects on dentine characteristics.

Enamel and dentine are the major mineralised structures in teeth. Dentine is a quasi-hexagonally packed hydrated organic matrix divided broadly into intertubular (ITD) and peritubular (PTD) dentine (Mjör and Nordahl, 1996; Tjäderhane et al., 2009; Veis, 2003). ITD is composed of a hydroxyapatite-reinforced collagen type I matrix and a small percentage of non-collagenous proteins (Tjäderhane et al., 2009). The PTD is a densely mineralised proteolipid-phospholipid complex that is physically and visually different to ITD (Gotliv and Veis, 2008). Within a tooth, the organisation and relative distribution of ITD and PTD will vary (Mjör and Nordahl, 1996). The PTD surrounds dentine tubules (DTs) which are densely packed close to the pulp. The pulp contains a dynamic system of blood and lymphatic vessels that communicates with the general vascular and neural system through the root canals into the jawbone. Lining the pulp periphery, adjacent to dentine, odontoblasts extend cell processes, within networks of tubules, into the tooth (Couve et al., 2013). The network of main tubules in the centre of the tooth are close to each other and then fan out towards the dentine-enamel junction (Couve et al., 2013; Mjör and Nordahl, 1996). The aptly named ITD lies between tubules.

Like bone, dentine is a collagenous mineralised tissue (Landis et al., 1993; Landis et al., 1996). Unlike bone, dentine does not turn over as the progenitor cells, the odontoblasts, are post-mitotic (Couve et al., 2013). Approximal to the pulp, odontoblasts lay new dentine throughout the life of the individual (Couve et al., 2013). Within the tubules, the odontoblast processes extend to the dentine-enamel junction to deliver nutrients, provide cell-to-cell communication and deposit mineral, until hindered by cellular ageing or apoptosis (Couve et al., 2013; Li et al., 2018). Other influences that affect dentine mineral can include caries and genetic diseases to cause pathological modifications (Arnold et al., 2001; Blatz et al., 2019; Perdigao J, 2010). However, an understanding of sound tooth structure is essential to help differentiate normal from pathology, and it is unclear how dentine mineral density and distribution changes with age and site in sound teeth.

The study of hard biological tissue such as dentine can be a challenge to prepare for Transmission Electron (TEM) or Scanning Electron Microscopy (SEM) studies. Electron microscopy techniques require mineralised tissue to be resin embedded and cut into thin sections using a microtome (Denk et al., 2004). Microtome cutting and sample preparation for EM require multi-stage chemical fixation and embedding with mechanical slicing using a knife (Nalla et al., 2005). Previously, gallium (Ga) FIB has been used to mill mature and young dentine slices or 'lamellae' to observe in TEM (Porter et al., 2005). The ultrafine lamellae required for TEM (<100 nm) are challenging and time consuming to prepare and are only suitable to visualise small (<20 μm) site-specific regions of interest (Nalla et al., 2005; Porter et al., 2005). Additionally, Ga can implant in substrates and introduce several artefacts (Rubanov and Munroe, 2004). Studies of Ga FIB-TEM lamellae have detected differences in crystal size between the dentine mineral in mature and young teeth (Porter et al., 2005), but could not correlate these findings beyond the levels of ITD and PTD as TEM lamellae are only for high-resolution imaging and cannot show changes across larger areas (>20 μm). In addition to using a Ga FIB-SEM for TEM lamellae preparation, a Xe Plasma FIB-SEM can be used to collect 3D volumes of dentin (Earl et al., 2010). Xenon is a heavier and larger ion than Ga allowing it to sputter more material. However, the collection and data analysis of 3D volumes is lengthy and time consuming so should only be attempted if volume data is required. Therefore, milling targeted large area (100 μm) cross-sections inside an SEM with a Xenon Plasma Focussed Ion Beam (Xe PFIB-SEM) is an alternative, less procedural method of observing mineralised tissue at the microscale (Earl et al., 2010). In Xe PFIB-SEM, it is easy to target a particular dentine tubule of interest to directly cross-section in order to collect high-resolution secondary electron micrographs to observe its morphology without the need to expose the sample to chemical etching or fixation.

To study broad changes to dentine mineral at the microscopic scale, SEM offers surface characterisation of dentine at high resolution (up to

1 nm per pixel) to provide an overview of dentine site dependent changes with age. Energy Dispersive X-ray Spectroscopy in the SEM (SEM-EDS) can be used to perform qualitative compositional analysis to identify elements present in a sample, while Integrated Mineral Analysis (TIMA) collects semi-quantitative data to identify the mineral phases present in samples at high resolution (1–2 μm). Backscattered Electron (BSE) micrographs collect information based on z-contrast (atomic number) and density. Heavier elements or relatively dense materials appear brighter than light elements and less dense or amorphous materials (Lloyd, 1987). Therefore SEM-EDS and TIMA can identify mineral phases present in material and BSE micrographs can provide high-resolution information on the material density to complement Xe PFIB-SEM data. Machine learning techniques can be applied to BSE images to segment and compare micrographs based on greyscale values (Arganda-Carreras et al., 2017; Schindelin et al., 2012).

The aim of this exploratory study was to determine the effect of patient age (young or mature), anatomical location (shallow or deep dentine and central or peripheral dentine) and microscopic site (ITD or PTD) on dentine mineral distribution, density and composition. Dentine morphology and microstructure was investigated by milling targeted cross-sections and collecting high-resolution secondary electron micrographs using a Xe PFIB-SEM. Backscattered electron (BSE) micrographs combined with Energy Dispersive X-ray Spectroscopy in the SEM (SEM-EDS) and TIMA were used to investigate qualitively the density, composition, and distribution of apatite. The BSE micrographs were further were analysed using machine learning to investigate dentine tubule distribution and changes to apatite density.

Materials & methods

Teeth extraction

Sound extracted human molars or premolars were collected from individuals who were medically fit to undergo oral surgery. A total of four teeth each were collected from 'Young' (19–20 years) and 'Mature' (54–77 years) patients (Fig. 1 A & Table A.1). Teeth collected for this project were free of caries and other pathology. Ethics approval for the project was granted by The University of Queensland's Institutional Human Research Ethics Approval Committee (Approval Number 2019000532). Extracted teeth were stored in phosphate buffered saline at 4 °C, and sterilised using gamma radiation prior to preparation. A high speed water-cooled dental hand piece (NSK S-Max M600L Nakanishi Inc. Japan) fitted with a coarse diamond bur was used to cut the teeth. Each tooth was sectioned in half to reveal the dentine-enamel junction (DEJ) and the pulp roof margin. Shallow slices were prepared 0.5–0.75 mm below the DEJ and deep slices 0.5–0.75 mm above the pulp roof (Fig. 1 A). The slices were washed and dried in ambient conditions and prepared for further analysis. For each slice, data was collected from the central and peripheral dentine locations (Fig. 1 G i). The effects of age and anatomical location on DTs, PTD and ITD observed in BSE and Xe PFIB-SEM micrographs were determined and analysed.

Xenon plasma focussed ion beam scanning electron microscopy (Xe PFIB-SEM) cross-sections of dentine tubules

Dentine slices previously used for SEM-EDS analysis (see below) were sectioned into smaller cubes and attached to 13 mm SEM aluminium stubs using silver paint and adhesive carbon tape before coating with 2 nm platinum using a Leica ACE EM600 coater. Two tooth slices were cross-sectioned using a Tescan Xe PFIB-SEM at a central inner dentine site (Fig. 2). Cross-sections 100 μm across were milled at a tilt of 55° using 30 kV. A current of 100nA was used to mill a trench in front of the cross-section roughly 150 μm in length, 75 μm wide and 50 μm in depth (Fig. 2 A). A beam current of 30nA was used to polish the surface of the cross-section (150 μm length × 3 μm width × 100 μm depth). The Xe PFIB-SEM micromanipulator needle was fitted with a single crystal
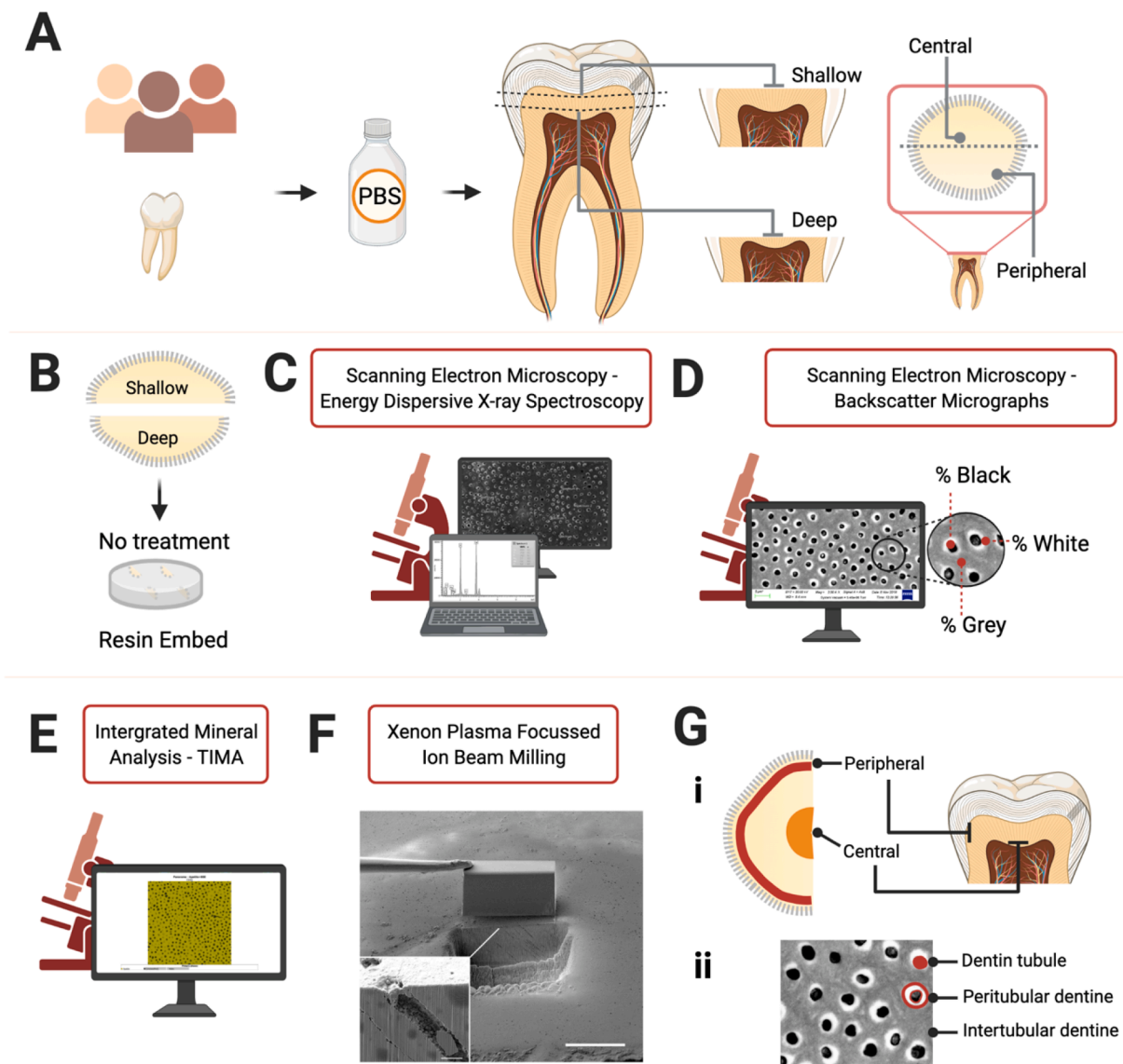
Fig. 1. A. Sound molar teeth were collected and immediately stored in Phosphate Buffered Saline. Teeth were hemi-sectioned to locate the dentine-enamel junction (DEJ) and pulp roof and prepared to shallow (0.5–0.75 mm below the DEJ) or deep (0.5–0.75 mm above the roof of the pulp) sites. **B.** A shallow and deep section was prepared from each tooth, dried in ambient conditions before resin embedding. **C.** Scanning Electron Microscopy and Energy Dispersive X-ray Spectroscopy identified elemental composition of peritubular and intertubular dentine. **D.** Backscattered Electron Micrographs analysed for percentage black, white & grey as well as relative grey intensity. **E.** Integrated Mineral Analysis of a young and mature tooth dentine was performed **F.** Xenon Plasm Focussed Ion Beam was used to mill dentine **G. i**. Depicts the sub-regional classification of central and peripheral dentine **ii**. The microscopic sites analysed in this study include dentine tubules, peritubular and intertubular dentine.

silicon mask (Fig. 2 A). The mask was located over the tooth site of interest to protect it from beam damage and to create a smooth flat surface during polishing (Fig. 2 A-E). Micrographs were collected using the secondary electron detector at 2 kV and 50 pA beam current (1024 × 1024 pixels). The Xe PFIB-SEM micrographs were assessed for internal and external tubule shape/morphology as well as ITD and PTD characteristics.

Scanning electron microscopy of dentine

Dentine slices (Table A.1) were embedded in 30 mm round pucks (Fig. A.1) using EpoFix resin (Struers), polished to a 1 μm finish, and coated in 10 nm carbon using a Cressington Carbon Coater. The BSE micrographs were collected for each tooth slice at three central and three peripheral dentine sites (N = 96) using 20 kV, a 30 μm aperture, and high current mode on a Zeiss Sigma VP field emission SEM.

Surface micrographs of unpolished teeth slices (Table A.1) were also collected using the secondary electron detector at 3 kV on a Tescan MIRA 3 field emission SEM. Each tooth slice was attached to a 13 mm SEM aluminium stub using adhesive carbon tape before coating with 2 nm platinum using a Leica ACE EM600 coater.

The BSE micrographs were collected to provide information based on z-contrast (atomic number) and density in polished dentine slices. A representative selection of BSE micrographs from a young person and a mature person were compared qualitatively to illustrate the effect of anatomical location and microscopic site on DT appearance as well as ITD and PTD characteristics. All BSE micrographs were also analysed by means of a two-step process that involved machine learning using Trainable Weka and Fast Random Forest classifier (Arganda-Carreras et al., 2017). Firstly, in batches of images, a trainable Weka segmentation tool within FIJI (Schindelin et al., 2012) was used to locate 'white', 'black' and 'grey' regions. Finally, all segmented images were processed
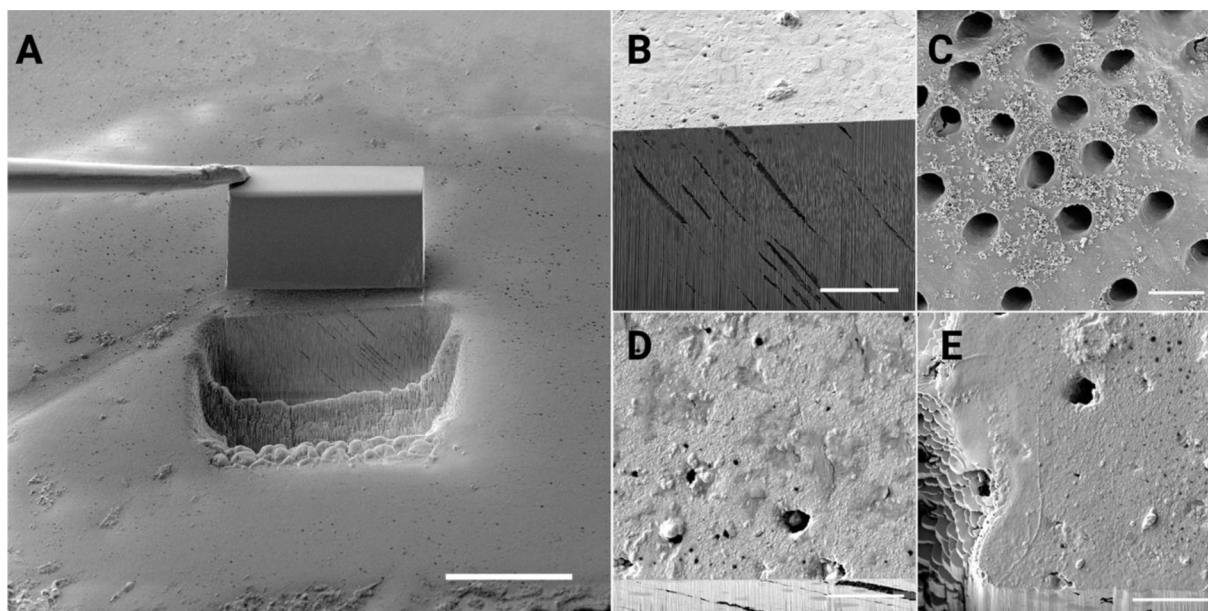
Fig. 2. Scanning electron micrographs of xenon plasma focussed ion beam (Xe PFIB-SEM) milling of tooth surface to create a cross-section of dentine tubules. **A.** Manipulator needle attached to a single crystal silicon mask (100 μm × 50 μm × 50 μm) held over the surface of a polished tooth slice to mill a flat surface using focussed xenon ions. **B.** Figure 'a' magnified to show the surface of the tooth and the cross-section after removal of the mask. **C.** The surface of the dentine from a tooth slice before embedding and polishing. **D.** The 'top' surface view of the polished tooth after milling. **E.** The 'top' surface of the polished surface after milling at the edge of the mask. The left hand side of this micrograph shows the pillaring effect from the xenon beam if a mask is not used. Scale bars = A. 100 μm, B. 20 μm, C-E. 5 μm.

using a second macro to quantify percentage area of each label, 'white', 'black' and 'grey' as well as the relative grey intensity values. The percentage areas for white, black and grey were used to determine the ratio of ITD (grey) to DTs (black), the relative number of DTs (black) and ITD grey intensity for patient age, anatomical location and microscopic site.

The analysis of the BSE results were performed on a data set collected from a small population. The use of the data was maximised by not collapsing data at the individual level and applying data in raw form by not averaging across values. Collapsing data or using averaged values can reduce the effect of individual variation. The analyses performed accounted for correlation between individual samples to generate models and the use of median, rather than average values.

Initial statistical analysis revealed there was strong evidence that the three outcome variables: ratio of ITD to DTs, relative number DTs, and ITD intensity, were not normally distributed as determined using quantile plots. Median regression with bootstrapping to account for the multiple measures per sample was used to model the ratio of ITD to DTs; and ITD intensity with an interaction term between age (young or mature) and location within the tooth (shallow central, shallow peripheral, deep central, and deep peripheral). As the relative amount of PTD was indicated by the number of DTs, a negative binomial regression model with clustered robust standard errors was used to estimate the effect of the predictor variables age and location.

Postestimation of marginal effects was used to estimate median and 95% confidence intervals (95% CI) for the median regression models and relative number ratios for the negative binomial regression at combinations of age and location. Model coefficients were tested using Wald tests. Factorial contrasts tested combinations of age and locations relative to other levels within each model. Stata (StataCorp, 2015) was used for analysis.

Energy dispersive X-ray spectroscopy of dentine

For each tooth slice (n = 16) (Table A.1), SEM-EDS was used to investigate dentine at three PTD and three ITD sites at both central and peripheral dentine. The SEM-EDS point analysis function was performed using 20 kV, a 30 μm aperture, and high current mode on a Zeiss Sigma VP field emission SEM equipped with a 50 mm^2 Oxford EDS detector. A total of 12 point spectra were collected per tooth slice along with BSE micrographs. The x-ray detector was calibrated to collect the same number of x-rays at each point (300,000). The SEM-EDS data was presented as averaged values for anatomical location and microscopic site.

Integrated mineral analysis was used to perform elemental mapping of the surface of one mature and one young tooth at shallow and deep locations in central and peripheral sites. Data was collected with a TIMA combined with two integrated SEM-EDS detectors in high-resolution mapping mode at 25 kV, ~8nA, and 15 mm working distance. Standard BSE detector and probe current calibrations were performed by the TIMA. Strength of BSE signal collected by the detector was used to determine which pixels in each 50 μm^2 panel EDS spectra were collected from. The bottom 15% darkest pixels are excluded in order to avoid collecting spectra from the EpoFix resin or in dentine tubules. The top 10% pixels are excluded to avoid collection in areas that were charging due to the electron beam. Pixel size was 100 nm^2 with 2500 x-rays collected at each pixel. The final dataset was 100 μm × 100 μm made up of four individual panels of 50 μm each. Data was analysed using TIMA software.

Results

Xe PFIB-SEM micrographs reveals nanoscale tubule and intertubular dentine structure

Three representative cross-sections of tubules were selected to illustrate key anatomical features (Fig. 3). The Xe PFIB-SEM micrographs presented here reveal PTD, DT and ITD in the transverse (Fig. 3 A), longitudinal (Fig. 3 B) and oblique planes (Fig. 3 C). In all planes, the ITD was nanoporous with voids within the mineralised collagenous matrix (Fig. 3 A–C) and appear to seamlessly integrate to PTD.

The DT observed in the transverse horizontal plane (Fig. 3 A) from a mature person has broad PTD perimeter with evidence of smaller
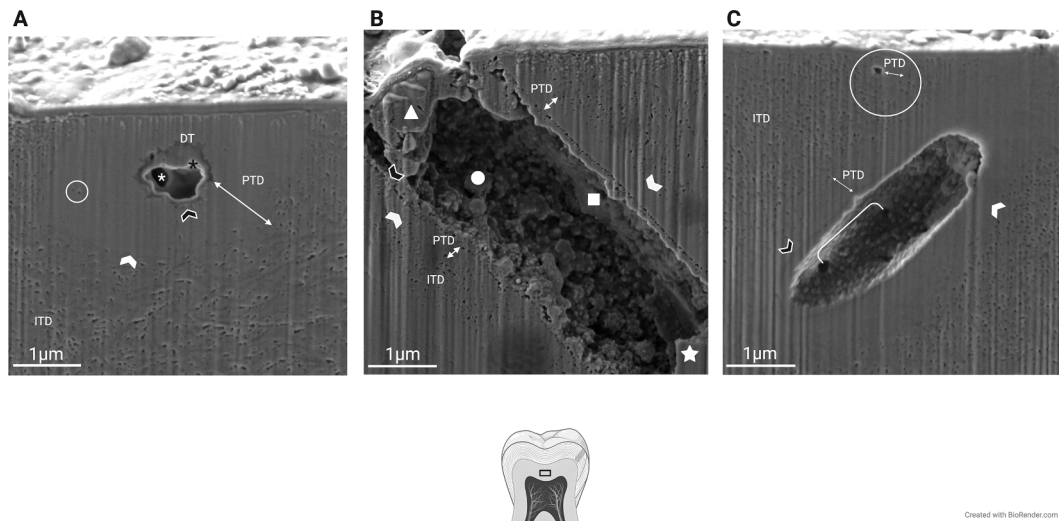
Fig. 3. Xenon Plasma Focussed Ion Beam Scanning Electron Microscopy (Xe-PFIB SEM) micrographs of dentine tubules (**DT**) from shallow central dentine from a **A.** mature person in transverse plane, a **B.** young person in longitudinal plane and a **C.** young person in an oblique plane. Micrographs reveal the location of the peritubular dentine (**PTD**) with the tips of the **double-ended arrows** demarcating PTD thickness, nanoporous intertubular dentine (**ITD**) with smaller tubules in cross-section (**circles**). A **white arrow** delineates the ITD from the PTD and a **black arrow** reveals the intersection between the PTD wall and the internal mineral architecture that has detached due to dehydration and resulting shrinkage. **A.** In the mature dentine cross-section, a **black asterisk** differentiates the original DT margin from internal calcifications and the unfilled tubule centre (**white asterisk**). **B.** The young dentine tubule in longitudinal cross-section depicts a **white triangle** where debris blocks the tubule entrance. Internally, a **white circle** identifies round deposits that line the lower tubule wall and a **white square** is located where material has formed against the superior wall. The PTD wall cross-section (**white star**) remains intact. **C.** The DT from a young person in oblique cross-section with smaller accessory tubules (**white bracket**) appears to originate from the main tubule.

tubules in cross-section within the PTD. There is an integrated uniform interface between ITD and PTD, unlike the homogenous mineral-like mass within the tubule lumen, which is well delineated from the PTD (Fig. 3 A DT: black asterisk) and the internal margins of the unfilled tubule (Fig. 3 A white asterisk).

A DT from a young person is viewed in the longitudinal plane (Fig. 3 B). The tubule entrance is blocked by dentine debris (Fig. 3 B white triangle). The left-hand side internal wall is lined by what could be round-shaped deposits (Fig. 3 B white circle). The superior wall of the tubule is adapted with what appears to be elongated flat deposits (Fig. 3 B white square) and a segment from the preserved PTD wall remains (Fig. 3 B white star). The potentially mineralised mass within the tubule has separated from the margins of the PTD (Fig. 3 B). The tubule has ITD on either side, as well as the PTD of the adjacent tubule visible in the high-resolution micrograph.

The tubule from a young person is presented in the oblique plane (Fig. 3 C). The micrograph reveals smaller tubules that appear to connect from within the major tubule in cross-section (Fig. 3 C). The PTD that surrounds a smaller accessory tubule shows evidence for centrally deposited mineral within its lumen (Fig. 3 C circle). Within the lumen of the larger main tubule, multiple smaller tubules appear to integrate to the PTD of the major tubule (Fig. 3 C bracket).

SEM BSE Micrographs

Qualitative analysis of BSE micrographs

A total of ninety-six BSE micrographs were analysed in this study (Young = 48; Mature = 48). A randomly selected panel of micrographs for a (young) 18-year-old (Fig. 4 A) person and a (mature) 63-year-old (Fig. 4 B) person is organised according to anatomical location. Cross-sectioned DTs from peripheral locations were oval-shaped (Fig. 4 A ii & iii; B ii & iii) and central locations, circular, to reflect the angle of the tubules (Fig. 4 A i & iii; B i & iii). The width of the young PTD walls appeared to vary with sparse mineral within the tubules. (Fig. 4 A). In mature dentine, the thickness of the PTD walls was relatively broader to surround mineral occluded tubule lumens (Fig. 4 B). In young dentine, the DT branches were dark with less mineral incorporated, unlike

mature dentine where the dentine tubules were filled (Fig. 4 A v and Fig. 4 B v).

Machine learning analysis

Tables 1–3 allow for direct comparisons between anatomical location, microscopic site and age. The superscript letters after each result allow for direct comparison between the different variables. When comparing different ages, sites and locations, results that do not share the same superscript letter are statistically significant and sharing one or more letters indicates no significant difference. All sites with no superscript letters reported were not statistically significantly different to any other site.

For instance there is a greater effect for the ratio of intertubular dentine to dentine tubule surface area (Table 1) in young deep central dentine (5.9 (–4.6, 16.4)[A]) compared with young deep peripheral dentine (71.6 (39.8, 103.3)[D]), but not mature deep central dentine (9.3 (–1.9, 20.4)[AB]).

Machine learning analysis of BSE micrographs shows spatial effects on ITD and DT presentation

The percentage areas of ITD to DT were compared. Spatially, dentine depth and site, but not age, had a greater effect on the ITD/DT ratio (P-value = 0.024) (Table 1). Deep central dentine scored the lowest ratio while shallow peripheral, the greatest (Fig. 5). There are relatively more DTs in deep central dentine while shallow peripheral dentine had less of an effect on DT numbers; the opposite is true for ITD.

Machine learning analysis of BSE micrographs shows relative number of dentine tubules affected by Age, site and location

The relative number of DTs showed a greater effect by location (P-value < 0.001) and age (P-value = 0.013) (Table 2). Per field of view, the least number of tubules was detected in young deep peripheral regions while deep central dentine for both age groups accounted for the greatest number of DTs (Fig. 5).

Intertubular dentine intensity differs by age, site and location

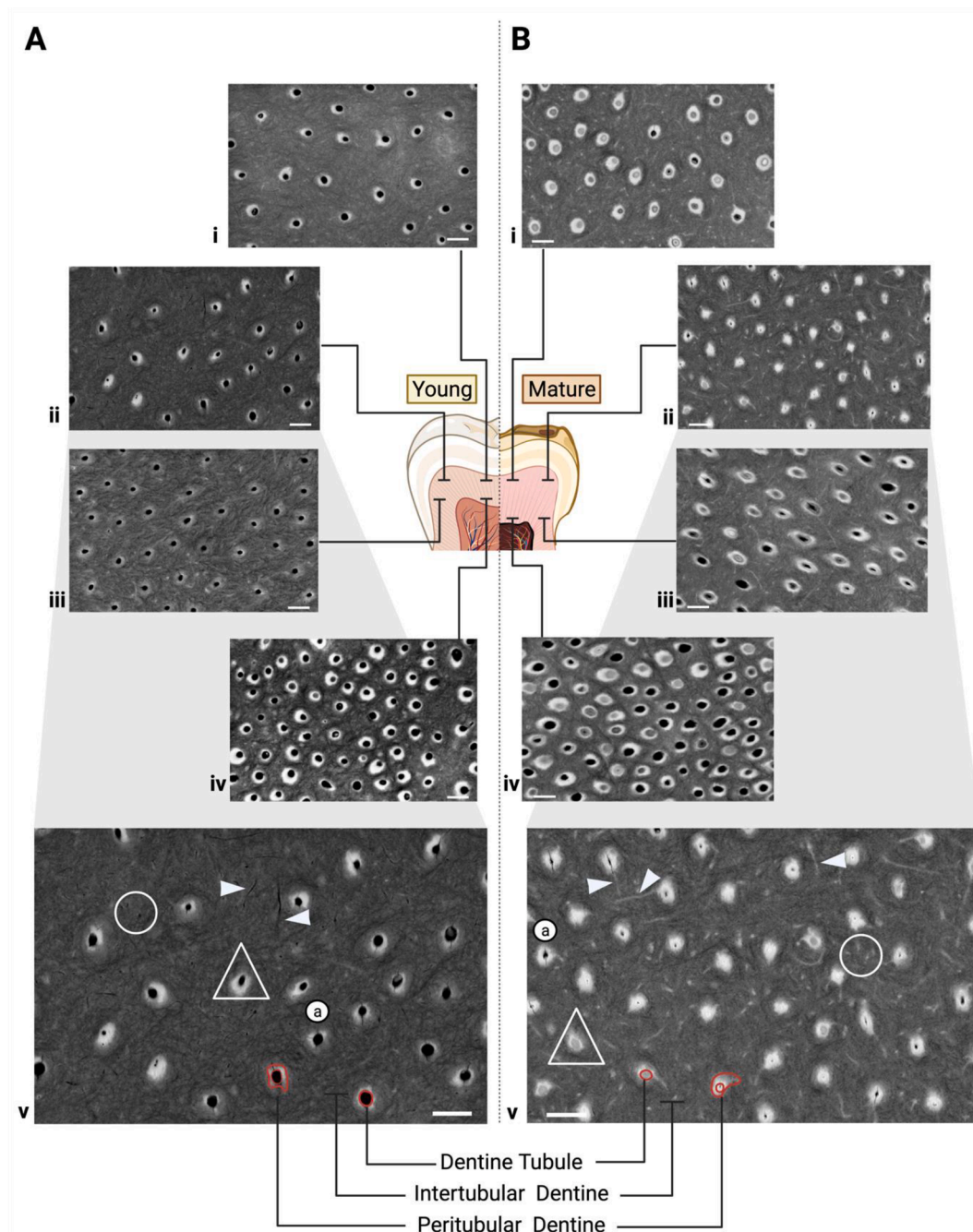Grey intensity values were measured for each micrograph. Relatively

Fig. 4. Scanning electron microscopy backscattered electron micrographs of polished dentine surfaces in the transverse plain from **A.** young 18-year-old and **B.** mature 63-year-old. Micrographs are shown for **i.** shallow peripheral **ii.** shallow central **iii.** deep peripheral and **iv.** deep central locations. **Av.** and **Bv.** are magnified versions of Aii. and Bii. respectively. Note the major dentine tubule branches in longitudinal views (**white arrows**) and transverse views (**circles**). The intact tubules in transverse view are visible (**triangle**) and intertubular dentine weave more prominent. Dentine tubules with dehydration cracks traversing through lie below **a.** Note the micrographs in Panel B are relatively lighter in intensity with more grey/white regions compared with Panel A. Scale bar = 5 μm.

high intensity measures (dark grey) represented less mineral dense surfaces while low values (light grey) indicated the presence of mineral. The ITD grey intensity varied by location (P-value = 0.046) and age (P-value = 0.5) (Table 3). Young shallow central dentine showed a greater effect for grey intensity (dark grey) to indicate less mineral at this site relative to mature shallow peripheral and deep dentine (light grey). Overall, the young dentine showed a greater effect on grey intensity measures than dentine in mature shallow peripheral regions (Fig. 5), to indicate lower mineral densities in ITD, PTD and DTs.

Qualitative elemental analysis using SEM-EDS and semi-quantitative integrated mineral analysis

Mineral detection (Apatite) by age, site and location

The SEM-EDS point analysis determined that all dentine locations contained calcium (Ca), phosphorus (P) and apatite (Tables B.1 & C.1). The individual x-ray counts of Ca and P for each surface, as well as the Ca/P ratio, were similar for the age groups and locations except for centrally located mature PTD, where the weight percentage (wgt%) of Ca was lower compared with all other sites (Tables B.1 & C.1). In addition to Ca and P (Fig. 6), O, Na, Mg, and Cl were detected as well

Table 1
Ratio of intertubular dentine to dentine tubule surface area by age and location.

Location	Median ratio of intertubular dentine to dentine tubule lumens (95% CI)	
	Young	Mature
Shallow Central	29.6 (0.2, 59.0)[BC]	76.2 (−20.4, 172.8)
Shallow Peripheral	69.3 (24.8, 113.9)[D]	82.1 (−302.0, 466.2)
Deep Central	5.9 (−4.6, 16.4)[A]	9.3 (−1.9, 20.4)[AB]
Deep Peripheral	71.6 (39.8, 103.3)[D]	46.8 (8.7, 84.8)[CD]

*Margins sharing a letter show values are not significantly different at a type one error rate of 0.05 while controlling for the field of view.
Model: P-value (Location) = 0.024; P-value (Age) = 0.37; P-value (Location*Age) = 0.38; Model R-square = 0.10.

Table 2
Relative number of dentine tubules with reference to young deep peripheral dentine adjusted for field of view.

Location	Relative number of dentine tubules (95% CI)	
	Young	Mature
Shallow Central	1.61 (0.90, 2.88)[AB]	1.71 (1.10, 2.66)[ABC]
Shallow Peripheral	1.05 (0.64, 1.71)[AB]	1.21 (0.93, 1.57)[AB]
Deep Central	2.50 (1.61, 3.87)[CD]	2.96 (2.31, 3.80)[D]
Deep Peripheral	1.00 *(Reference)*[A]	1.57 (1.10, 2.25)[BC]

*Margins sharing a letter show values are not significantly different at a type one error rate of 0.05 while controlling for the field of view.
Model: P-value (Location) < 0.001; P-value (Age) = 0.013; P-value (Location*Age) = 0.68; Model R-square = 0.09.

Table 3
Median SEM BSE micrograph relative intensity (degree of mineralisation) by age and location within the tooth.

Location	Median intertubular dentine intensity (95% CI)	
	Young	Mature
Shallow Central	156 (107, 204)[C]	105 (86, 124)[ABC]
Shallow Peripheral	156 (95, 216)[BC]	90 (76, 104)[A]
Deep Central	101 (46, 157)[AB]	97 (87, 107)[AB]
Deep Peripheral	129 (78, 181)[AC]	103 (93, 114)[AB]

*Margins sharing a letter show values are not significantly different at a type one error rate of 0.05 while controlling for the field of view.
Model: P-value (Location) = 0.046; P-value (Age) = 0.05; P-value (Location*Age) = 0.13; Model R-square = 0.30. High intensity = less mineralisation. Low intensity values = greater mineralisation.

(Tables B.1 & C.1). Element map data collected using the TIMA identified that apatite distribution extends from ITD to within the PTD to indicate mineral inclusion within the tubules, while no mineral was detected inside the young dentine tubules. Additional elements including Mg and Na were also detected in the TIMA (Fig. B.1).

Discussion

Physiological ageing increases dentine apatite density and distribution, but not composition. Dentine apatite density and distribution varies with anatomical location and microscopic site observed. The Xe PFIB-SEM micrographs show architecturally different, yet seamless integration of DTs to ITD. The SEM BSE micrographs illustrated apatite imbued mature DTs with branching extending into ITD. Analysis of the BSE micrographs indicated an overall increase in mineral density for mature dentine, compared with young, in PTD and branches within ITD. Within the tubules, the mineral density was greatest in mature deep central dentine where the margins between the ITD, PTD and DT contents were indistinguishable in the TIMA scans for Ca, P and apatite. While the DTs showed signs of mineral apposition with age, the Xe PFIB-SEM characterised ITD to remain structurally consistent for age and

observation plane. The changes to mineral density observed in the SEM BSE micrographs are likely due to age-related apatite deposition within the main tubules, with particular emphasis on the mineral-filled branches that extend within ITD. The mineral characteristics of ITD depend on tubule density and BSE micrograph analysis indicated tubule dense regions to have less ITD and vice versa. Spatially, analysed BSE micrographs depicted the number of DTs to be greatest in deep central dentine and lowest in shallow peripheral regions. Conversely, ITD surface area was highest in shallow peripheral dentine and lowest in deep central dentine. The ITD in shallow peripheral dentine will present with increased branching between the DTs; these branches eventually fill with mineral as a person ages, to increase mineral density within mature ITD.

Functioning odontoblast cells and processes deposit mineral within the tubules (Couve et al., 2013; Li et al., 2018). Li et al. (2018) demonstrated the odontoblast process to extend from the cell body adjacent to the centrally located pulp, within the tubule, to span the length of the tooth where it terminates at the dentine-enamel junction. Mjör and Nordahl (1996) identified DT branches of varying diameters that extended from the main tubule into ITD. In dentine, tubule branches include major (0.5–1.0 mm diameter), fine (300–700 nm) and micro dentine branches (25–200 nm) (Mjör and Nordahl, 1996). Previously, mineral deposition was believed to be limited to within the main DT lumens (Li et al., 2018). Mineral deposits within the tubule branches in the mature BSE dentine micrographs suggest the odontoblast processes extend not only the length of the tooth within the DTs, but also into the branches that spread in ITD. Yet, the ITD remains structurally similar regardless of spatial orientation or age. The age-related increase in mineral density may be attributed to apatite within the branches that populate ITD.

Within the young tubules, the presence of variably sized, shaped and spaced structures thought to be calcospherites (Chu et al., 2010; Mishima and Kozawa, 1998) appeared to follow typical crystal nucleation processes (Landis et al., 1996). While the possible calcospherites varied in diameter and height, the small and larger spherical crystals appeared to fuse with time to form large co-planar aligned mineral platelets (Landis et al., 1993). Over time, continuous mineral seeding, apposition and crystal nucleation occludes the main tubules and their branches (Couve et al., 2013; Li et al., 2018; Tjäderhane et al., 2009; Weber, 1974). In this study, evidence of mineral seeding was observed in the Xe PFIB-SEM micrographs of young dentine and the mineral platelets appeared to coalesce into a homogenous mass within mature tubules. The mineral mass appeared structurally distinct from the PTD and ITD in the Xe PFIB-SEM micrographs of young and mature DTs. These formations inside the tubules are believed to be natural structures as any redeposition of milled material following cross-sectioning with the Xe beam occurs to the sides and front of milled cross-sections.

The architectural difference between ITD, PTD and the apatite deposits within DTs suggests unique mineralisation processes (Porter et al., 2005). Compared with ITD, the mineral deposits within the tubules lack the scaffolding of the ITD collagen matrix skeleton (Tjäderhane et al., 2009), and the PTD proteolipid-phospholipid concentricity (Gotliv and Veis, 2008). A previous Ga FIB-SEM TEM lamellae study noted nanostructural differences in mineral deposits between the ITD and within tubules (Porter et al., 2005). The tubule contents were described as a polycrystalline mineral produced by heterogenous nucleation of hydroxyapatite precipitate (Porter et al., 2005). In contrast, the smaller plate-like crystals in ITD were polarised and surrounded by an amorphous collagen matrix (Porter et al., 2005; Tjäderhane et al., 2009). The same study measured a relative reduction in crystalline size in mature compared with young ITD. The authors hypothesised that mineral dissolution reduced crystal size within ITD to reprecipitate within the tubule lumens (Porter et al., 2005). According to the Xe PFIB-SEM micrographs, the architecture of ITD appears to remain consistent with age as well as observation plane. While there is a possibility of mineral reprecipitating into the tubule lumens, odontoblast process activity may
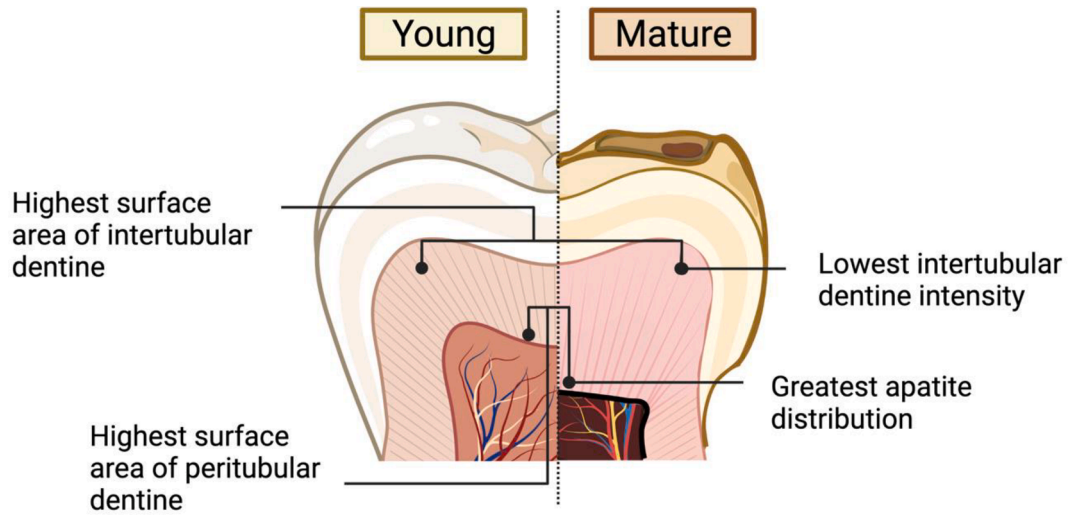
Fig. 5. Summary of major findings for Scanning Electron Microscopy backscattered electron micrograph analysis and Energy Dispersive X-ray results for young and mature dentine at shallow and deep, central and peripheral locations.
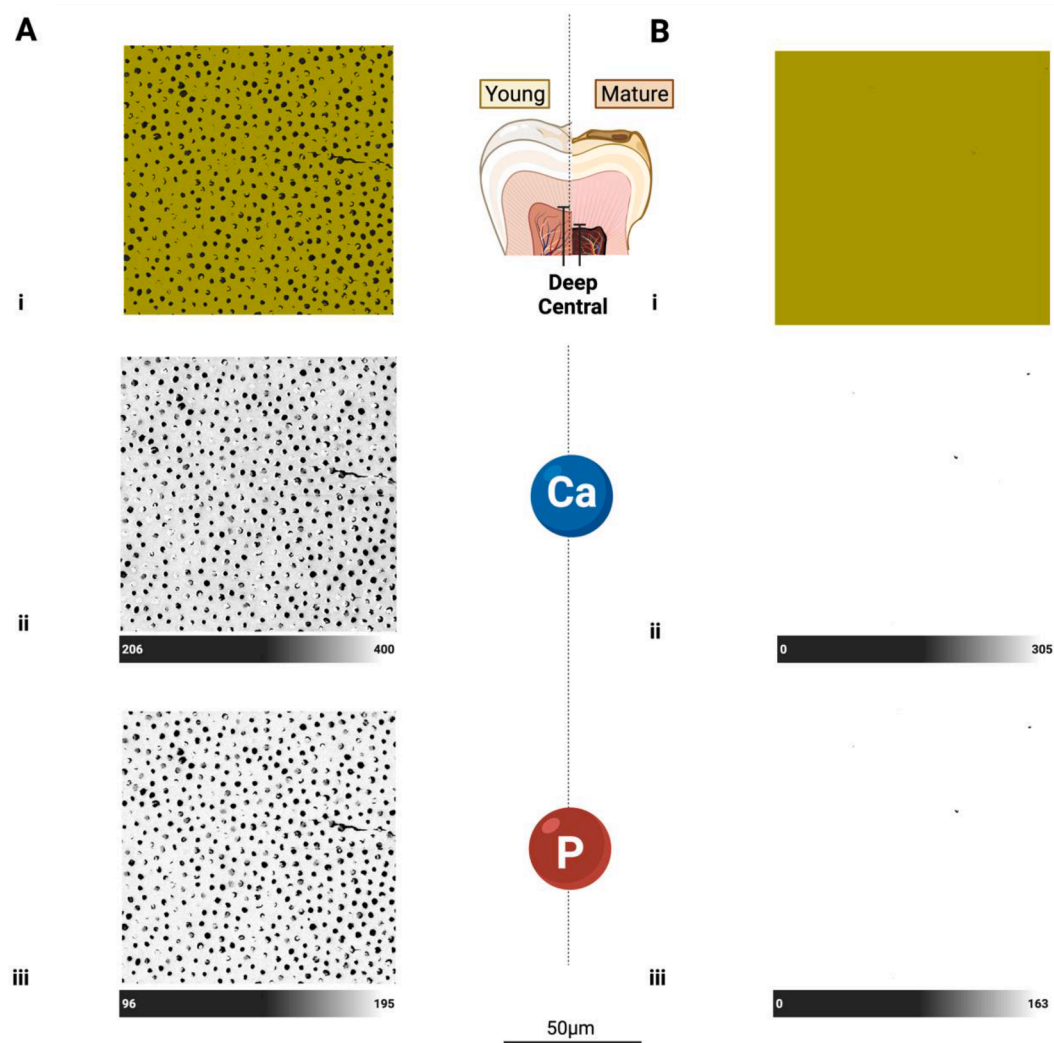

Fig. 6. Panel of elemental and phase maps from Scanning Electron Microscopy Integrated Mineral Analysis (TIMA) deep central dentine surfaces in the transverse plane from a **A.** young and **B.** mature person. Maps are shown for **i.** Apatite **ii.** Calcium **iii.** and Phosphorus. Below each Calcium and Phosphorus map is a scale that indicates the number of x-rays identified at each pixel (2500 x-rays were collected at every pixel). Scale bar = 50 μm.

also play a pivotal role in mineral apposition (Couve et al., 2013; Li et al., 2018).

Continuous mineral apposition in DTs by odontoblast processes is attributed to mineral occlusion inside the tubule lumens (Couve et al., 2013; Li et al., 2018). Open, unfilled mature DTs observed in BSE micrographs are likely a result of compromised odontoblast activity (Weber, 1974). Aged yet viable odontoblasts may continue to seed and nucleate mineral in centripetal apposition against the internal PTD walls of the main tubules and their branches (Arnold et al., 2001; Veis, 2003; Weber, 1974). The centripetal mineral apposition theory is supported by the increase in mineral density, measured in mature dentine BSE micrographs, as well as the change in appearance of the cross-sectioned tubule lumens for young compared with mature tubules in the Xe PFIB-SEM micrographs.

While age, location and site affected mineral distribution and density, dentine mineral composition remained stable. The TIMA and SEM-EDS results confirmed the presence of Ca and P across the anatomical locations, microscopic sites and age groups. The Ca/P ratios collated for young dentine in this study were in accordance with previous findings (Arnold et al., 2001; Mlakar et al., 2014). The detection of sodium and chloride may be a consequence sample storage in saline. Traces of magnesium were also detected in all regions with both TIMA and SEM-EDS, although in a previous study only hydroxyapatite, not magnesium, was detected (Porter et al., 2005). In dentine, magnesium substitutes tricalcium phosphate to form stable ß-TCMP or Magnesium-Whitlockite that is commonly associated with physiological ageing (LeGeros et al., 1995). However, the detection limit of SEM-EDS is roughly 1–1.5 wgt% and further studies are required to quantify and measure change to composition including Mg or other elements across the changing surface of dentine (Hodoroaba, 2020). The detection of magnesium in this study would require further analysis.

Changes to dentine trace elements would be a useful addition to the current body of knowledge. Both SEM-EDS and TIMA identify amorphous and crystalline material yet cannot detect trace elements or associate elements with the apatite mineral. Future analyses could include the use of an Electron Probe Microanalyser (EPMA) that applies wavelength dispersive spectroscopy in the SEM and offers quantification of trace elements (0.01–0.04 wgt%) (Lanari et al., 2019). However, EPMA experiments can be time consuming, reducing the capacity for large sample numbers. Another technique to consider in future studies is Laser Ablation Induction Coupled Plasma Mass Spectroscopy (LA-ICP-MS), which can detect trace elements present in parts per billion (Heinrich et al., 2003). Although LA-ICP-MS investigates areas about 50 μm across, which would make it difficult to compare ITD with PTD.

Various methods were selected to study the effects of age, anatomical location and microscopic site on dentine mineral density and distribution. The combination of SEM-EDS, TIMA, BSE images and Xe PFIB-SEM cross-sectioning to reveal high-resolution morphology of polished dentine provided interdependent supportive data. The BSE micrographs exhibit changes in apatite density across the surface of the dentine that is supported by the SEM-EDS and TIMA analysis, which identify the material as apatite. The BSE images were analysed using machine learning for microstructure and distribution of DTs and ITD as well as grey scale values to represent apatite density. The grey scale values are largely indicative of mineral (Ca/P) content as the low atomic number of C, H, and O would make up the remainder of the dentine material. The Xe PFIB-SEM removed the need for complex, multi-stage specimen preparation to investigate cross-sections of targeted dentine, to reduce artefacts yet yield high resolution surface images.

Conclusion

Physiological ageing increased dentine mineral density by changing mineral distribution while apatite composition remains the same. Dentine mineral apatite is deposited within the tubules and branches that fenestrate into ITD. Within a tooth, apatite distribution will depend on the anatomical location (central or peripheral in shallow or deep) and microscopic site (ITD or PTD).

Declaration of Competing Interest

The authors declare that they have no known competing financial interests or personal relationships that could have appeared to influence the work reported in this paper.

Appendix A. Supplementary data

Supplementary data to this article can be found online at https://doi.org/10.1016/j.yjsbx.2022.100060.

References

Arganda-Carreras, I., Kaynig, V., Rueden, C., Eliceiri, K.W., Schindelin, J., Cardona, A., Sebastian Seung, H., Murphy, R., 2017. Trainable Weka Segmentation: a machine learning tool for microscopy pixel classification. Bioinformatics 33 (15), 2424–2426.

Arnold, W.H., Konopka, S., Gaengler, P., 2001. Qualitative and Quantitative Assessment of Intratubular Dentine Formation in Human Natural Carious Lesions. Calcif. Tissue Int. 69, 268–273.

Arola, D., Reprogel, R., 2005. Effects of aging on the mechanical behavior of human dentin. Biomaterials 26 (18), 4051–4061. https://doi.org/10.1016/j.biomaterials.2004.10.029.

Bajaj, D., Sundaram, N., Nazari, A., Arola, D., 2006. Age, dehydration and fatigue crack growth in dentine. Biomaterials 27 (11), 2507–2517.

Blatz, M.B., Chiche, G., Bahat, O., Roblee, R., Coachman, C., Heymann, H.O., 2019. Evolution of aesthetic dentistry. J. Dent. Res. 98 (12), 1294–1304.

Chu, C.-Y., Kuo, T.-C., Chang, S.-F., Shyu, Y.-C., Lin, C.-P., 2010. Comparison of the microstructure of crown and root dentine by a scanning electron microscopic study. J. Dent. Sci. 5, 14–20.

Couve, E., Osorio, R., Schmachtenberg, O., 2013. The amazing odontoblast: activity, autophagy, and aging. J. Dent. Res. 92 (9), 765–772.

Denk, W., Horstmann, H., Kristen M. Harris, 2004. Serial block-face scanning electron microscopy to reconstruct three-dimensional tissue nanostructure. PLoS Biology 2 (11), e329.

Earl, J.S., Leary, R.K., Perrin, J.S., Brydson, R., Harrington, J.P., Markowitz, K., Milne, S. J., 2010. Characterization of dentinee structure in three dimensions using FIB-SEM. J Microsc 240, 1–5.

Eltahlah, D., Lynch, C.D., Chadwick, B.L., Blum, I.R., Wilson, N.H.F., 2018. An update on the reasons for placement and replacement of direct restorations. J. Dent. 72, 1–7.

Gotliv, B.A., Veis, A., 2008. The composition of bovine peritubular dentine: Matching TOF-SIMS, scanning electron microscopy and biochemical component distributions – New light on peritubular dentine function. Cells Tissues Organs 189, 12–19.

Heinrich, C.A., Pettke, T., Halter, W.E., Aigner-Torres, M., Audétat, A., Günther, D., Hattendorf, B., Bleiner, D., Guillong, M., Horn, I., 2003. Quantitative multi-element analysis of minerals, fluid and melt inclusions by laser-ablation inductively-coupled-plasma mass-spectrometry. Geochimica et Cosmochimica Acta 67 (18), 3473–3497.

Hodoroaba, V.-D., 2020. In: Characterization of Nanoparticles. Elsevier, pp. 397–417. https://doi.org/10.1016/B978-0-12-814182-3.00021-3.

Lanari, P., Vho, A., Bovay, T., Airaghi, L., Centrella, S., 2019. Quantitative compositional mapping of mineral phases by electron probe micro-analyser. Geological Society, London, Special Publications 478 (1), 39–63.

Landis, W.J., Song, M.J., Leith, A., McEwen, L., McEwen, B.F., 1993. Mineral and organic matrix interaction in normally calcifying tendon visualized in three dimensions by high-voltage electron microscopic tomography and graphic image reconstruction. J. Struct. Biol. 110 (1), 39–54.

Landis, W.J., Hodgens, K.J., Song, M.J., Arena, J., Kiyonaga, S., Marko, M., Owen, C., McEwen, B.F., 1996. Mineralization of collagen may occur on fibril surfaces: evidence from conventional and high-voltage electron microscopy and three-dimensional imaging. J. Struct. Biol. 117 (1), 24–35.

LeGeros, R.Z., Kijkowska, R., Bautista, C., Legeros, J.P., 1995. Synergistic Effects of Magnesium and Carbonate on Properties of Biological and Synthetic Apatites. Connect Tissue Res 33 (1-3), 203–209.

Li, C., Jing, Y., Wang, K., Ren, Y., Liu, X., Wang, X., Wang, Z., Zhao, H., Feng, J.Q., 2018. Dentinal mineralization is not limited in the mineralization front but occurs along with the entire odontoblast process. Int. J. Biol. Sci. 14 (7), 693–704.

Lloyd, G.E., 1987. Atomic number and crystallographic contrast images with the SEM: a review of backscattered electron techniques. Mineral. Mag. 51 (359), 3–19.

Mishima, H., Kozawa, Y., 1998. SEM and EDS analysis of calcospherites in human teeth. Eur. J. Oral Sci. 106 (S1), 392–396.

Mjör, I.A., Nordahl, I., 1996. The density and branching of dentinal tubules in human teeth. Arch. Oral Biol. 41 (5), 401–412.

Mlakar, N., Pavlica, Z., Petelin, M., Štrancar, J., Zrimšek, P., Pavlič, A., 2014. Animal and human dentine microstructure and elemental composition. Open Medicine (Warsaw, Poland) 9, 468–476.

Müller, F., Shimazaki, Y., Kahabuka, F., Schimmel, M., 2017. Oral health for an ageing population: the importance of a natural dentition in older adults. Int. Dent. J. 67, 7–13.

Nalla, R., Porter, A., Daraio, C., Minor, A., Radmilovic, V., Stach, E., Tomsia, A., Ritchie, R., 2005. Ultrastructural examination of dentine using focused ion-beam cross-sectioning and transmission electron microscopy. Micron 36, 672–680. https://doi.org/10.1016/j.micron.2005.05.011.

Perdigao, J., 2010. Dentine bonding-variables related to the clinical situation and the substrate treatment. Dent Mater 26, e24–37. https://doi.org/10.1016/j.dental.2009.11.149.

Porter, A.E., Nalla, R.K., Minor, A., Jinschek, J.R., Kisielowski, C., Radmilovic, V., Kinney, J.H., Tomsia, A.P., Ritchie, R.O., 2005. A transmission electron microscopy study of mineralization in age-induced transparent dentine. Biomaterials 26 (36), 7650–7660. https://doi.org/10.1016/j.biomaterials.2005.05.059.

Rubanov, S., Munroe, P.R., 2004. FIB-induced damage in silicon. J. Microsc. 214 (3), 213–221. https://doi.org/10.1111/j.0022-2720.2004.01327.x.

Schindelin, J., Arganda-Carreras, I., Frise, E., Kaynig, V., Longair, M., Pietzsch, T., Preibisch, S., Rueden, C., Saalfeld, S., Schmid, B., Tinevez, J.-Y., White, D.J., Hartenstein, V., Eliceiri, K., Tomancak, P., Cardona, A., 2012. Fiji: an open-source platform for biological-image analysis. Nat. Methods 9 (7), 676–682. https://doi.org/10.1038/nmeth.2019.

StataCorp. 2015. Stata 14.2, College Station, Texas, USA.

Tjäderhane, L., Carrilho, M.R., Breschi, L., Tay, F.R., Pashley, D.H., 2009. Dentine basic structure and composition-an overview. Endod Topics 20, 3–29. https://doi.org/10.1111/j.1601-1546.2012.00269.x.

Veis, A., 2003. Mineralization in organic matrix frameworks. Rev. Mineral. Geochem. 54, 249–289. https://doi.org/10.2113/0540249.

Weber, D.F., 1974. Human dentine sclerosis: A microradiographic survey. Arch Oral Biol 19, 163,IN111,169-168,IN112,169 , 10.1016/0003-9969(74)90211-8.